Selective oligosaccharide recognition with phenylboronic acid through Cu(I)-catalysed click imprinted surfaces

Norman, J.; Tommasone, S.; Mendes, P.m.

DOI:
10.1016/j.mtchem.2022.100939

Document Version
Publisher's PDF, also known as Version of record

Citation for published version (Harvard):
Norman, J, Tommasone, S & Mendes, PM 2022, 'Selective oligosaccharide recognition with phenylboronic acid through Cu(I)-catalysed click imprinted surfaces', *Materials Today Chemistry*, vol. 24, 100939. https://doi.org/10.1016/j.mtchem.2022.100939

Materials Today Chemistry 24 (2022) 100939

Contents lists available at ScienceDirect

Materials Today Chemistry

journal homepage: www.journals.elsevier.com/materials-today-chemistry/

Selective oligosaccharide recognition with phenylboronic acid through Cu(I)-catalysed click imprinted surfaces

J. Norman, S. Tommasone, P.M. Mendes*

School of Chemical Engineering, University of Birmingham, Edgbaston, Birmingham, West Midlands, B15 2TT, UK

ARTICLE INFO

Article history:
Received 1 February 2022
Received in revised form
31 March 2022
Accepted 5 April 2022
Available online 14 May 2022

Keywords:
Molecular imprinting
Copper(I)-catalysed click reaction
Saccharide recognition
Boronic acid
Self-assembled monolayers

ABSTRACT

With the emerging role of glycans as potential diagnostic markers of disease, highly selective diagnostic platforms must be developed to realise the clinical value of irregular glycan expression patterns. Overcoming chemical and structural homogeneity between oligosaccharide structures however remains a significant challenge, which largely rests on the capability to develop materials embedding precise carbohydrate recognition. Herein we report a surface imprinting strategy that takes advantage of the high yield Cu(I)-catalysed azide-alkyne cycloaddition (CuAAC) click reaction to achieve oligosaccharide imprinted cavities featuring precisely organized phenylboronic acid (PBA) motifs. Central to the construction of the imprinted surface was the choice of a foundation alkyne-terminated monolayer of a long alkyl chain to impart a high surface click efficiency of the PBA motif. By pre-forming and clicking an oligosaccharide:PBA complex onto the alkyne-terminated monolayer and capping the free space, selective oligosaccharide imprinted cavities were formed with low millimolar dissociation constants.

1. Introduction

Producing a clinically relevant assay for selective quantification of specific oligosaccharides remains a major challenge in the development of novel prognostic and diagnostic tests for detection of aberrant glycosylation as instigated in numerous diseases, including cancer [1–5], autoimmune [6,7], neurodegenerative [8] and cardiovascular conditions [9]. The currently used techniques including lectins and anti-glycan antibodies suffer from inherent low selectivity and specificity imparted by the subtle differences and poor immunogenicity of saccharide ligands [10–12], while more sensitive techniques such as mass spectroscopy require complex sample work-up methods unsuited to clinical settings [13–17].

Offering a completely synthetic route, molecular imprinting is a promising development in the diagnostic industry, using ligand template driven synthesis of a functional binding cavity on a substrate expressing selected binding motifs. This allows pragmatism in design approach of artificial receptors exhibiting a tailored network of hydrogen bonding [18,19], van der Waals [20], electrostatic [21], hydrophobic [22–24] or covalent interaction [25–27] (or combination thereof [28–31]) within the polymer. Providing a combination of covalent, ionic or hydrogen bonding interactions, boronic acid (BA) has been deployed as a functional monomer for various ligands including proteins, neurotransmitters and glycans [32–34]. Cyclic esterification of BA through 1,2 or 1,3 *cis*-diols produces a reversible pH sensitive covalent bond thus provides a unique characteristic of the designed imprints allowing easy removal of template ligand and regeneration of the binding pocket for multiple uses. Furthermore, pH dependency allows modification of binding affinity where pH > pKa of the PBA consistent with hybridization of the boron constituent from sp2 trigonal planar to sp3 tetrahedral anionic configuration [35].

Affinity between BA and several amino acids provides a platform for imprinting of proteins, relying on a large network of weak multivalent interactions during imprinting [36,37]. Imprints selective for proteins, including horseradish peroxidase and haemoglobin, have been developed in a microplate format, in which the selectivity was shown to be dependent on both BA and polymer chain spatial orientation while affinity was also affected by template charge *i.e.* positively charged proteins did not form imprints with BA [33]. The importance of spatial constraints and binding pocket formation on ligand rebinding was further reported by imprinting various structural isoforms of β-lactoglobulin (BLG) using 3-aminophenylboronic acid (APBA) as the functional monomer [36]. Selectivity was observed for imprinted native isoforms

* Corresponding author.
E-mail address: p.m.mendes@bham.ac.uk (P.M. Mendes).

https://doi.org/10.1016/j.mtchem.2022.100939

over non-native BLG, confirming ligand conformation significantly affects re-binding affinity.

Targeting 1,2 or 1,3 *cis*-diols, BA additionally shows high affinity for catechol group containing neurotransmitters including dopamine, epinephrine, and norepinephrine. Early imprinting designs used a simple oxidation grafting of APBA in solution with template epinephrine to polystyrene microplate wells showing increased affinity for imprints at higher pH due to covalent bond formation [38]. This was later expanded to include 3-thiopheneboronic acid during imprinting which used in combination with APBA produced selective imprints for the herbicide atrazine demonstrating expanded potential for target ligands [34]. Targeting dopamine with APBA, increased selectivity was shown over similar compounds *.i.e.* epinephrine, via inclusion of vinyl groups within the imprinting cavity, providing enhanced mass transfer/binding kinetics at the surface-liquid interface [39]. The application of BA to MIPs is however uniquely suited to binding of saccharides imparted by their abundance of suitable *cis*-diols seeing use in imprints for saccharide antibiotics [40], monosaccharides [26,41] and glycoprotein biomarkers [25,27,42]. Providing a highly controllable reaction, atom transfer radical polymerisation (ATRP) has been used to produce selective MIPs for glycoproteins [25,42]. For instance, RNAse B imprinted surfaces with complementary binding pockets based on BA motifs have shown selectivity for RNAse B over de-glycosylated counterpart RNAse A and, α1-acid glycoprotein and horseradish peroxidase (HRP) [25].

The sensitivity and selectivity of any imprinted surface will naturally derive from successful coupling of functional monomers to the base self-assembled monolayer (SAM), hence regioselective, high yield and biologically compatible coupling reactions are essential. The Cu(I)-catalysed azide-alkyne cycloaddition (CuAAC) provides almost exclusively 1,4 disubstituted triazoles through reaction of azides with alkynes and can be adapted for both aqueous and organic solvent conditions [43–46]. Furthermore, no cross-reactivity is observed for glycan structures thus it provides a promising candidate for oligosaccharide sensing BA functional surfaces. Despite high surface yields previously reported for CuAAC functionalized surfaces, it has not yet been applied to BA-based imprints [47,48].

To this end, we introduce the design and realization of an oligosaccharide specific binding cavity expressing complimentary PBA binding motifs using a template-driven Cu(I)-catalysed azide-alkyne cycloaddition (CuAAC) click reaction (Fig. 1). The approach utilizes an alkyne-terminated SAM on gold to couple via the CuAAC reaction with a pre-formed oligosaccharide-PBA complex, enabling precise PBA surface spatial arrangement. The immobilized complex is subsequently used to create the complementary molecular shape on the surface using azido-heptaethylene glycol (azOEG) moieties. Removal of the oligosaccharide leaves behind the selective oligosaccharide imprinted cavities.

2. Results and discussion

Primarily, our first objective was to produce a stable alkyne-terminated SAM with high organization. Given the discordant yields of the CuAAC reaction previously reported for SAM functionalization ranging between 7 and 80% [48–50], optimization of the composition of the SAM molecule was necessary to improve surface yield of the PBA units, SAM packing density, organization and reduce defect formation [51–55]. To this end, three SAM molecules were synthesized (supporting information), providing a short (C_3Alkyne), branched (C_{br}Alkyne) and long (C_{11}Alkyne) composition (Table 1). These SAM molecules were selected based on the monomer structure impact on packing density and organization allowing optimization of surface PBA yield post CuAAC reaction.

SAMs were prepared by immersing gold substrates in piranha solution for 7 min after which, substrates were rinsed and immersed in 0.1 mM methanolic solutions of C_3Alkyne, C_{Br}Alkyne or 0.2 mM C_{11}Alkyne for 24 h under argon, providing sufficient time for formation of the gold-thiolate bond between each monomer and the Au substrate [56,57]. SAM composition and packing was monitored by ellipsometry, contact angle and X-ray photoelectron spectroscopy (XPS).

Both C_3Alkyne and C_{br}Alkyne SAMs produced low SAM packing and disorganized monolayers, presenting lower than expected thickness and advancing contact angle (θ_{Adv}) and high Au_{4f}/S_{2p} ratios as determined by XPS (Table 1). Ellipsometry and contact angle measurements of the C_{11}Alkyne SAM show a consistent and expected thickness (1.81 ± 0.04 nm) and θ_{Adv} (82.6 ± 2.3°), accordant with terminal alkyne groups [56] and low hysteresis (5.7°), demonstrating high organization of this monolayer. Chemisorption of the thiol group to the Au substrate was confirmed by XPS with a doublet peak detected at 162.2 eV ($S_{2p2/3}$) and 163.4 eV ($S_{2p1/2}$) and the C_{1s}, O_{1s} and N_{1s} species also confirmed (supporting information). Elemental ratios of N_{1s}:S_{2p}, O_{1s} and C_{1s} showed consistency with the chemical composition of C_{11}Alkyne (Table 1), confirming formation of the C_{11}Alkyne SAM. Interestingly, both C_3Alkyne and C_{br}Alkyne SAMs showed increased propensity for contamination over the C_{11}Alkyne SAM, with C_{1s} spectra consistently showing significant adventitious carbon for C_3Alkyne and C_{br}Alkyne monolayers. Furthermore, attempts at functionalization with azPBA were unsuccessful as confirmed by XPS for C_3Alkyne and C_{br}Alkyne with no B_{1s} peak detected. Significant Cu_{2p} contamination was also present for C_3Alkyne attributed to copper contamination from the CuAAC catalyst. As this was not observed on C_{11}Alkyne and C_{br}Alkyne, this suggests Cu(I) chelation is likely not occurring at exposed alkyne groups. From these initial studies, it was possible to conclude that both C_3Alkyne and C_{br}Alkyne monolayers provided poor foundations for azPBA functionalization and thus they were excluded from further developments.

To demonstrate the utility of the CuAAC reaction in producing saccharide imprinted surfaces, we then pursued the *in situ* azPBA addition to prepared C_{11}Alkyne SAMs (C_{11}Alkyne-azPBA). For comparison purposes, a SAM was also prepared by first coupling via the CuAAC reaction the C_{11}Alkyne moiety with 3-azidomethylphenyl boronic acid (azPBA) in solution, followed by SAM formation. Successful coupling on the C_{11}Alkyne-azPBA SAM was confirmed with the increased film thickness from 1.81 ± 0.04 nm to 2.54 ± 0.04 nm and a decrease in θ_{Adv} (67.2 ± 2.7°) (Table 2). Successful cycloaddition of the azPBA groups was confirmed by XPS with observation of triazole N═N at 402.7 eV in N_{1s} spectra, PBA hydroxyl groups at 532.9 eV in O_{1s} spectra and the presence of an attenuated peak in B_{1s} spectra at 192.2 eV (supporting information).

Surface yield of PBA groups on the C_{11}Alkyne-azPBA was determined through N/S ratio where 100% yield would provide a 4:1 N/S ratio as shown in Table 2. After 4 h (N/S ratio 2.3 ± 0.2), no further addition of PBA groups is observed on the surface with no increase observed after 18 h reaction (N/S ratio 2.3 ± 0.2). Only a small increase in N/S ratio is seen after 1 h (N/S ratio 1.8 ± 0.2), suggesting the reaction is mostly complete within the first hour. Increasing the concentration of azPBA in the reaction is not expected to increase yield where we expect steric hindrance of attached PBA groups to prevent further association of the Cu(I) catalyst with remaining alkyne groups thus markedly reducing reaction rate [57]. Examination of bound ($S_{2p3/2}$ 162.2 eV, $S_{2p1/2}$ 163.4 eV) and unbound (163.7 $S_{2p3/2}$, 164.9 eV $S_{2p1/2}$) sulphur showed an average unbound sulphur of 45.1 ± 2.6% across all reaction time intervals. Surprisingly, SAM organization appears

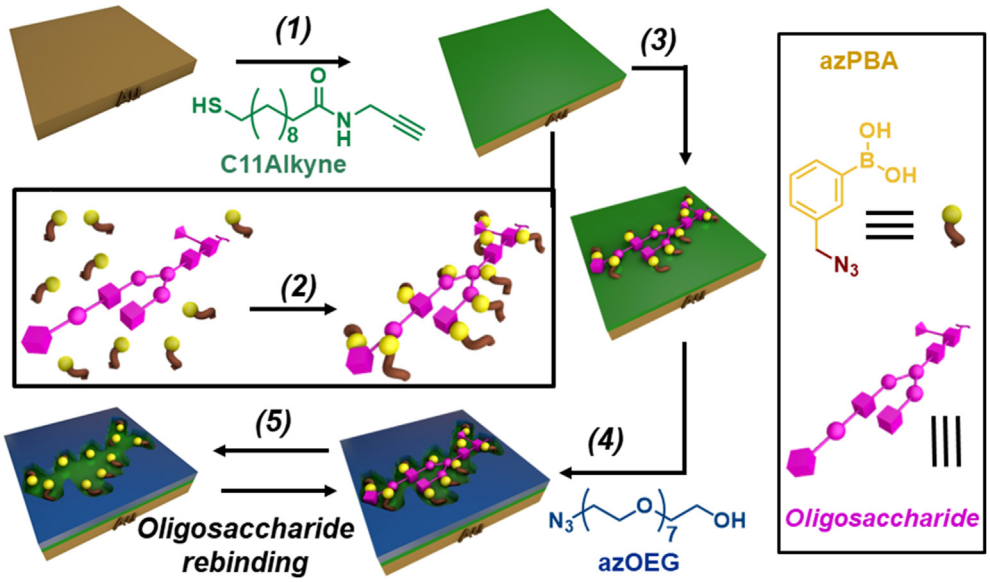

Fig. 1. Overview of the oligosaccharide imprinted surface synthesis: (*1*) Alkyne-terminated SAM formation on gold; (*2*) Reversible complexation of the azPBA saccharide binding unit to the template oligosaccharide; (*3*) surface immobilization of azPBA:oligosaccharide complex to the alkyne-terminated SAM via CuAAC reaction; (*4*) cavity formation using azOEG providing an inert anti-fouling layer and binding pocket; (*5*) removal of the template oligosaccharide.

Table 1
Ellipsometric thickness, advancing and receding water contact angles, and XPS elemental ratios for the C_3Alkyne, C_{br}Alkyne and C_{11}Alkyne SAMs. Theoretical thickness values were determined using ChemDraw3D (ver. 19.1).

SAM precursor	Ellipsometric thickness (nm)		Contact angle (°)			XPS elemental ratios	
	Theor.	Measured	Adv (θ_{Adv})	Rec (θ_{Rec})	Hys (θ_{Hys})	Theor.	Measured
C_3Alkyne 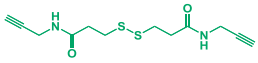	0.73	0.40 ± 0.03	78.6 ± 1.0	65.0 ± 2.0	13.6	N/S − 1 N/O − 1 C/N - 6 Au/S − n/a	0.8 ± <0.1 [a] [a] 24.9 ± 0.8
C_{br}Alkyne 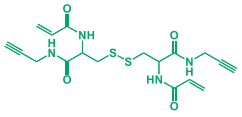	0.73	0.49 ± 0.04	70.5 ± 3.0	56.4 ± 7.0	14.1	N/S − 2 N/O − 1 C/N − 4.5 Au/S − n/a	3.0 ± <0.1 2.9 ± 0.1 [a] 77.7 ± 15.3
C_{11}Alkyne 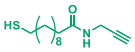	1.85	1.81 ± 0.04	82.6 ± 2.3	76.9 ± 1.9	5.7	N/S - 1 N/O - 1 C/N − 14 Au/S − n/a	1.4 ± 0.1 1.1 ± 0.1 13.8 ± 0.4 19.2 ± 1.5

[a] Ratios have been omitted due to atmospheric contamination providing unreliable fitting of elemental composition.

Table 2
Ellipsometric thickness, advancing and receding water contact angles, and XPS elemental ratios for the SAMs of C_{11}Alkyne-azPBA (azPBA coupled on the surface) and C_{11}Alkyne-Pre-azPBA (azPBA coupled in solution). For the C_{11}Alkyne-azPBA SAM, the CuAAC reaction was conducted for 1 h, 4 h and 18 h and the surface yields obtained based on the XPS elemental ratios. Theoretical thickness values were determined using ChemDraw3D (ver. 19.1).

SAM	CuAAC reaction	Ellipsometric thickness (nm)		Contact angle (°)			XPS elemental ratios		Yield (%)
		Theor.	Measured	Adv (θ_{Adv})	Rec (θ_{Rec})	Hys (θ_{Hys})	Theor.	Measured	
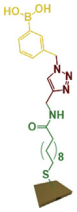	**Surface** C_{11}Alkyne-azPBA	2.64	2.54 ± 0.04	67.2 ± 2.7	58.7 ± 2.3	8.5	N/S − 4	*1h* 1.8 ± 0.2 *4h* 2.3 ± 0.2 *18h* 2.3 ± 0.2	26.8 ± 5.4 44.3 ± 5.7 41.7 ± 6.9
	Solution C_{11}Alkyne-Pre-azPBA	2.64	2.20 ± 0.10	74.5 ± 2.0	63.5 ± 2.8	11.0	N/S − 4	4.0 ± 0.6	–

reduced for the C_{11}Alkyne-Pre-azPBA showing deviation from expected values for both thickness (2.2 ± 0.10 nm) and θ_{Adv} (74.5 ± 2.0°) with an increase in hysteresis (11.0°). This was assigned to a limited number of inter backbone interactions from inclusion of bulky aromatic groups. XPS analysis of the C_{11}Alkyne-Pre-azPBA SAM confirms lower organization of the monolayer

showing both chemisorbed sulphur at 162.1 eV ($S_{2p2/3}$) and 163.3 eV ($S_{2p1/2}$) and unbound sulphur at 163.3 eV ($S_{2p2/3}$) and 164.5 eV ($S_{2p1/2}$) with significant adventitious carbon peak at 284.8 eV. Packing density is additionally decreased comparing the Au/S ratio from the C_{11}Alkyne (19.2 ± 1.5) to C_{11}Alkyne-Pre-azPBA (87.6 ± 16.9), suggesting inclusion of terminal aromatic groups inhibits dense surface packing. No B_{1s} species was detected ascribed to the low sensitivity of XPS for boron and the low surface concentration of C_{11}Alkyne-Pre-azPBA. Nonetheless, triazole N═N species peaks were observed in N_{1s} spectra (401.8 eV) alongside azPBA hydroxyl groups in O_{1s} spectra (532.9 eV), confirming presence of azPBA on the substrate. Derived elemental ratios of N/S and N/O are consistent with the chemical composition of the C_{11}Alkyne-Pre-azPBA monomer, confirming chemisorption of the C_{11}Alkyne-Pre-azPBA SAM to the gold substrate.

Saccharide affinity of the prepared C_{11}Alkyne-azPBA (1 h CuAAC reaction) and C_{11}Alkyne-Pre-azPBA SAMs was investigated using surface plasmon resonance (SPR) with spectra adjusted for removal of bulk refractive change using a benzyl azide functionalized C_{11}Alkyne SAM (C_{11}Alkyne-azBEN). Three monosaccharides, fructose, galactose and glucose, which are known to bind PBA with different affinities [26], were used at different concentrations (1.6 mM, 3.1 mM, 6.3 mM, 12.5 mM and 25 mM) to calculate the equilibrium dissociation constant (K_D) and surface saturation response, R_{max}. The K_D values were determined based on the SPR responses at equilibrium (R_{eq}), which were plotted against the concentration of injected monosaccharide (C) and fitted to a 1:1 steady-state affinity model. The model utilizes a nonlinear least-squares regression method to fit data to the Langmuir adsorption isotherm (Eq. (1)). The equation not only allows calculating K_D but also R_{max}.

$$R_{eq} = \left(\frac{C}{C + K_D}\right) R_{max} \quad (1)$$

As anticipated, monosaccharide-PBA affinity follows the pattern fructose>galactose>glucose for both the C_{11}Alkyne-azPBA and C_{11}Alkyne-Pre-azPBA SAMs (Fig. 2), showing significantly increased binding capacity (R_{max}) for fructose (206.8 ± 6.4 RU; 150.7 ± 6.4 RU) over glucose (124.2 ± 8.7 RU; 53.3 ± 4.9 RU) (Table 3). These results confirm the saccharide responsiveness of the PBA-terminated monolayers [58]. Surprisingly, C_{11}Alkyne-Pre-azPBA SAM affinity for fructose (2.8 ± 0.6 mM) was higher than for C_{11}Alkyne-azPBA counterpart (7.7 ± 0.7 mM) but showed decreased total binding capacity than C_{11}Alkyne-azPBA (206.8 ± 6.4 RU) (Table 3). Given the 26.8 ± 5.4% surface yield of azPBA on the C_{11}AlkyneSAM at 1 h, we can expect two scenarios: even spacing between PBA terminal groups arising from steric constraints on the Cu(I)-alkyne association during the CuAAC reaction thus inhibiting dense packing or alternatively; island formation of PBA groups arising from local presence of Cu(I) catalyst in the CuAAC reaction progression thus producing sterically unconstrained PBA groups at island step edges [49]. As affinity for C_{11}Alkyne-Pre-azPBA for fructose is increased over C_{11}Alkyne-azPBA and given the propensity for aromatic group containing SAMs to form nano-islands [59], this suggests the latter scenario; congregation of PBA groups in nano-islands with correlated PBA surface concentration to total binding capacity but sterically hindered thus reducing affinity. Conversely, reducing PBA surface concentration reverses this observation.

With an observed reaction yield of 41.7 ± 6.9% at 18 h and 26.8 ± 5.4% at 1 h, we have established the surface CuAAC reaction proceeds rapidly with diminished gains after 1 h. As we might expect template ligand dissociation from the functional PBA groups at longer incubation times, this rapid reaction progression is advantageous in maximising the azPBA:oligosaccharide complex

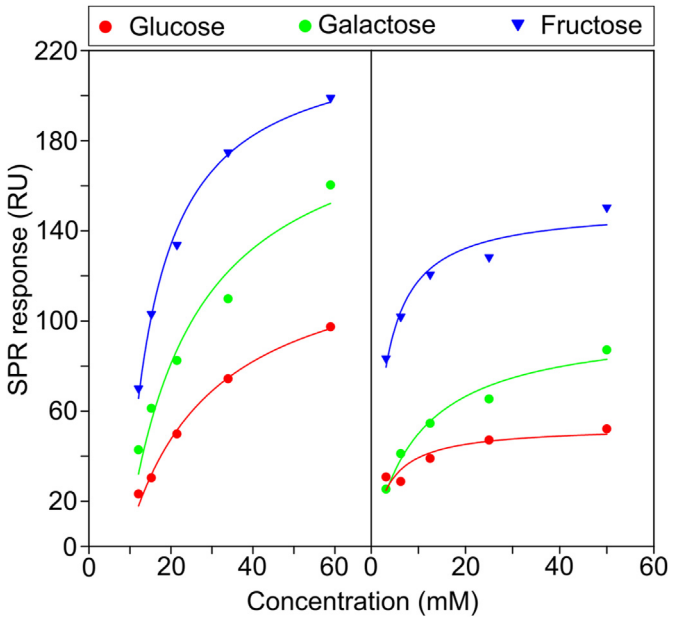

Fig. 2. SPR responses at equilibrium for the C_{11}Alkyne-azPBA (*left*) and C_{11}Alkyne-Pre-azPBA (*right*) SAMs versus the concentration (1.6 mM, 3.1 mM, 6.3 mM, 12.5 mM and 25 mM) of monosaccharide, fructose, galactose and glucose, from which K_D values have been obtained.

Table 3
SPR-derived K_D and R_{max} values for the C_{11}Alkyne-azPBA and C_{11}Alkyne-Pre-azPBA SAMs obtained using the monosaccharides, fructose, galactose and glucose.

	Monosaccharide	K_D (mM)	R_{max} (RU)	R^2
C_{11}Alkyne-azPBA	Fructose	7.7 ± 0.7	206.8 ± 6.4	0.98
	Galactose	16.6 ± 5.2	184.2 ± 24.2	0.94
	Glucose	20.7 ± 3.2	124.2 ± 8.7	0.99
C_{11}Alkyne-Pre-azPBA	Fructose	2.8 ± 0.6	150.7 ± 6.4	0.95
	Galactose	9.9 ± 2.1	99.4 ± 7.4	0.97
	Glucose[a]	3.5 ± 1.4	53.3 ± 4.9	0.82

[a] Low R^2 value will reflect low confidence in accurate K_D calculation as caused by low binding of PBA to particular monosaccharides i.e., glucose.

immobilization onto the surface. Furthermore, we have established a critical requirement for successful surface coupling based on the chemical composition of the base SAM, with the C_{11}Alkyne producing a densely packed monolayer with high surface organization thus providing our foundation SAM for imprinting.

Following the insights gained from the model monolayers above, studies proceed to generate oligosaccharide imprinted cavities onto C_{11}Alkyne SAMs. To demonstrate the viability of the approach, stachyose was selected as a model oligosaccharide due to its structural mimicry of the sugar chains of glycoproteins and easy availability. To create a stachyose specific molecularly imprinted surface, an azPBA:stachyose complex was synthesized as previously described by us [60], substituting benzoboroxoles for azPBA. C_{11}Alkyne SAMs were prepared on gold substrates as described above and subsequently immersed in a solution containing the azPBA:stachyose complex and the CuAAC catalyst in a 2:1 DMF:UP H_2O solution. To determine the optimum time for complex immobilization, C_{11}Alkyne SAMs were reacted for 1, 4, 8 and 24 h before being rinsed with HPLC MeOH. An inert scaffold was subsequently attached, surrounding the complex using azOEG, by submersing the C_{11}Alkyne:azPBA:stachyose complex substrates in a 1.6:1 DMF: UP H_2O solution of the CuAAC catalyst and azOEG (1 mM) for 24 h. The stachyose template was removed by sonicating the substrates in UP H_2O for 10 min followed by liberal rinsing hydrolysing the covalent BA-saccharide esters. In order to identify

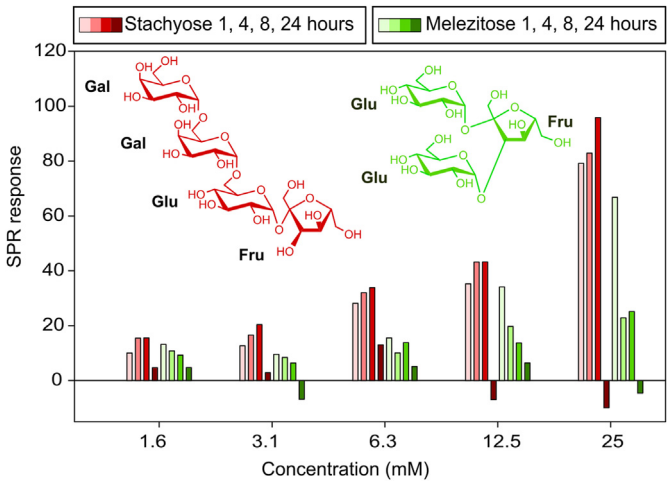

Fig. 3. SPR responses at equilibrium for the imprinted surfaces versus the concentration (1.6 mM, 3.1 mM, 6.3 mM, 12.5 mM and 25 mM) of oligosaccharide, stachyose (red gradient) and melezitose (green gradient). Different CuAAC reaction times (1 h, 4 h, 8 h and 24 h) were used for complex immobilization.

the properties imparted by the inclusion of azPBA and azOEG on the imprinted surfaces, the surfaces were characterized by ellipsometry and SPR before (complex only) and after azOEG incorporation.

Despite the low thickness of the complex only SAM compared to the theoretical (2.88 nm), an increase in thickness was observed over the base C_{11}Alkyne SAM (1.81 ± 0.04 nm) at each timed interval. As we expected a lower yield imparted by reduced azPBA concentration and increased steric constraints on the CuAAC reaction with the inclusion of stachyose, the thickness values support the successful immobilization of the azPBA:stachyose complex onto the C_{11} SAM albeit in lower concentration. Incorporation of the azOEG molecules further increased the film thickness, across each timed interval with increased film thickness observed at shorter reaction intervals. This suggests that at 1 h reaction, reduced azPBA:stachyose complex surface immobilization was achieved, leading to higher azOEG incorporation on the surface. These results are in agreement with the binding and selectivity of the imprinted surfaces as obtained by SPR (Fig. 3).

Since stachyose and melezitose are structurally related oligosaccharides, both containing a fructose and a glucose (β2-α1 glycosidic bond), melezitose was used as a control to evaluate selectivity. As shown in Fig. 3, selectivity for stachyose is enhanced with increased surface reaction times, reaching its maximum at 8 h. Despite earlier XPS studies showing a 26.8 ± 5.4% yield of azPBA on the C_{11}Alkyne SAM post CuAAC reaction, minimal selectivity was seen after 1 h of complex immobilization on the surface. These results are in agreement with ellipsometry data that also suggested incomplete azPBA:stachyose complex immobilization for 1 h CuAAC reaction. The reduced amount of azPBA carbohydrate receptors on the surface led to lower stachyose binding and poor discrimination between this oligosaccharide and melezitose. Increasing reaction time to 4 and 8 h significantly improved selectivity for stachyose over melezitose, suggesting both more complete complimentary PBA motif formation on the surface and increased surface concentration of PBA motifs. This is supported by the lower thickness of 8 h (2.28 ± 0.05 nm) imprinting over 4 h (2.78 ± 0.13 nm), where a reduction in surface azOEG is expected (Table 4). However, at longer reactions times (24 h) response to both saccharides were substantially decreased. This was ascribed to dissociation of the saccharide from the complex during the reaction, enabling both sporadic placement of the azPBA and azOEG groups.

Table 4
Ellipsometric thickness at each stage of the imprinting, starting with complex only on the surface, followed by azOEG incorporation and template removal. Different CuAAC reaction times (1 h, 4 h, 8 h and 24 h) were used for complex immobilization.

Surface reaction time (h)	Complex only (nm)	azOEG incorporation (nm)
1	1.96 ± 0.06	2.87 ± 0.16
4	2.04 ± 0.12	2.78 ± 0.13
8	2.09 ± 0.07	2.28 ± 0.05
24	2.24 ± 0.02	2.55 ± 0.05

With 8 h confirmed as the optimum imprinting time for inducing selectivity, evaluation of reproducibility and effect of the binding cavity on selectivity was then assessed. Two types of imprinted surfaces were produced using 8 h CuAAC reaction time, one surface only with the imprinted azPBA receptors (Step 3-Fig. 1) that lack the defined binding cavity formed by the OEG chains and another surface with the imprinted azPBA receptors and azOEG molecules. Selectivity was then gauged by exposure of the two imprinted surfaces to either stachyose or melezitose using SPR (Fig. 4). Selectivity was once more observed for both azOEG(−) and azOEG(+) surfaces for stachyose over melezitose. However, no significant difference in affinity was seen on inclusion of azOEG, with both surfaces showing similar K_D (azOEG(−) 17.8 ± 10.8 mM, azOEG(+) 14.9 ± 5.5 mM) (Table 5). Interestingly, inclusion of azOEG demonstrated lower deviation between replicates ascribed to either less stable inter-PBA motif stachyose binding on azOEG (−) surfaces or increased stability of stachyose binding on azOEG(+) surfaces produced from hydrogen binding sites presented on the azOEG chain within the cavity [61]. Comparison of the azOEG(+) imprinted surface to the C_{11}Alkyne-azPBA SAM showed comparable affinity and total binding capacity for stachyose (C_{11}Alkyne-azPBA K_D 11.3 ± 4.9 mM, R_{max} 125.8 ± 25.1; azOEG(+) imprinted surface 14.9 ± 5.5 mM; R_{max} 175.4 ± 33.2 RU) confirming no reduction in binding efficiency of PBA for stachyose between monolayers and imprints. Importantly, while the imprinted surfaces were shown negligible binding to melezitose, binding was observed to the C_{11}Alkyne-azPBA (K_D 22.6 ± 6.2 mM, R_{max} 143.5 ± 23.0). These experimental results showed that the spatial

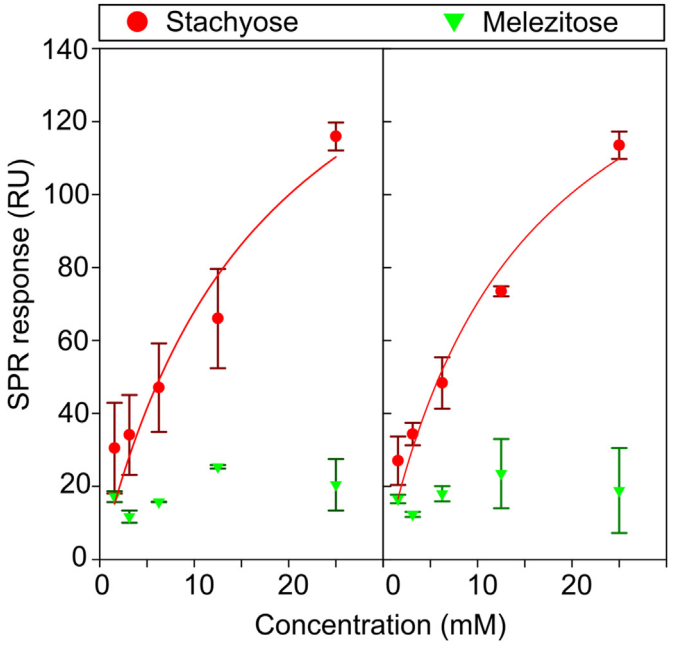

Fig. 4. SPR responses at equilibrium for the imprinted surfaces without (*left*) and with azOEG (*right*) incorporation versus the concentration (1.6 mM, 3.1 mM, 6.3 mM, 12.5 mM and 25 mM) of oligosaccharide, stachyose and melezitose.

Table 5
SPR-derived K_D and R_{max} values for the imprinted surfaces without and with azOEG incorporation obtained using stachyose. For comparison purposes, K_D and R_{max} values for the C_{11}Alkyne-azPBA using stachyose and melezitose are also shown.

	Oligosaccharide	K_D (mM)	R_{max} (RU)	R^2
Imprinted surface without azOEG	Stachyose	17.8 ± 10.8	188.8 ± 61.9	0.91
	Melezitose	–	–	–
Imprinted surface with azOEG	Stachyose	14.9 ± 5.5	175.4 ± 33.2	0.96
	Melezitose	–	–	–
C_{11}Alkyne-azPBA	Stachyose	11.3 ± 4.9	125.8 ± 25.1	0.91
	Melezitose	22.6 ± 6.2	143.5 ± 23.0	0.98

arrangement of the azPBA receptors is crucial to establish the selective binding for the target oligosaccharide. The K_D values obtained are in the low mM range, providing room for further affinity enhancements, which can potentially be achieved by expanding the precise spatial inclusion in the imprinting cavity of other residues known to interact with carbohydrates, such as tryptophan and tyrosine amino acids [62].

3. Conclusion

In conclusion, the unique characteristics of the Cu(I)-catalysed azide-alkyne cycloaddition (CuAAC) click reaction, such as high yield, high selectivity and compatibility with aqueous media, provided the foundation to develop an effective surface imprinting approach for selective oligosaccharide binding. Careful selection of the foundation alkyne SAM was shown to be fundamental for immobilization of the carbohydrate receptors (azPBA), with longer alkyl chains exhibiting greater surface reaction yields. Selectivity was provided by the spatial arrangement of the azPBA molecules on the surface, wherein an optimum CuAAC reaction time (8 h) was required to maximise the immobilization of a pre-made azPBA:oligosaccharide complex. Capping of the free space around the immobilized complex using azOEG had minimal effect on the binding properties, enhancing mainly the reproducibility of the formed cavities. The imprinted surfaces were capable of binding selectively oligosaccharides with low millimolar equilibrium dissociation constants, thereby opening up opportunities for their utilization in oligosaccharide-affinity materials for applications ranging from life sciences to diagnostics.

4. Materials and methods

4.1. Materials

Commercially available solvents were purchased from Sigma-Aldrich and used without further purification. All other chemicals and saccharides, with exception of those synthesized in house, were purchased from Sigma-Aldrich. SAMs used in SPR experiments were synthesized on polycrystalline gold substrates comprised of 50 nm gold on a thin layer (1 nm) of chromium (Reichert Technologies, USA). Alternatively, SAMs used for ellipsometry, contact angle and XPS experiments used a polycrystalline gold substrate containing a 100 nm layer of gold covering a 5 nm adhesion layer of chromium (George Albert PVD, Germany). ^{1}H and ^{13}C NMR spectra were recorded on a Bruker AVIII400 at 400 MHz and 101 MHz respectively at room temperature. All silica gel chromatography purification of SAM components used Sigma-Aldrich 60 A silica gel (35–70 μm).

4.2. Formation of C_{11}Alkyne and C_{11}Alkyne-Pre-azPBA SAMs on Au substrates

Au substrates were chemically cleaned using piranha solution (7:3, H_2SO_4, 30% H_2O_2) for 7 min before rinsing liberally with UP H_2O followed by HPLC grade MeOH and dried under an argon stream. Clean Au substrates were then immersed in degassed solution of C_{11}Alkyne (0.2 mM, 1 mL) in HPLC grade MeOH for 18 h on a rotary mixer. Following SAM formation, the substrates were liberally rinsed in HPLC grade MeOH and dried under an argon stream. Prior to C_{11}Alkyne-Pre-azPBA SAM formation, the acetate protecting group was removed. To a solution of acetate-C_{11}Alkyne-Pre-azPBA (0.26 mM, 3 mL) in EtOH, potassium hydroxide (0.8 mM, 1 mL) was added and the solution sonicated for 5 min then left for 2 h at room temperature on a rotary mixer. Post-deprotection, clean Au substrates were immersed in 1 mL of C_{11}Alkyne-Pre-azPBA solution and mixed for 18 h before liberal rinsing with EtOH and drying under argon.

4.3. Terminal modification of C_{11}SAMs with azPBA, azOEG or azBEN

C_{11}Alkyne SAMs were modified post-immobilization by CuAAC reaction with either 1 mM azOEG, 1 mM azPBA or 1 mM azBEN dissolved in a pre-prepared Cu(I) catalyst solution, which was prepared by stepwise addition of Cu(II)SO_4, sodium L-(+)-ascorbate (NaAsc) and tris(benzyltriazoleylmethyl)amine (TBTA) producing a final concentration of: azido ligand (1 mM), Cu(II)SO_4 (10 mol%), NaAsc (20 mol%) and TBTA (10 mol%). C_{11}Alkyne SAMs were immersed in 1 mL 1.6: 1 DMF:UP H_2O azido ligand/catalyst solution for 1 h on a rotary mixer and protected from light. The surface reaction was quenched by liberal rinsing of the substrates with 1:1 UP H_2O:HPLC MeOH, proceeded by sonication in this solution for 10 min. Substrates were rinsed a final time with HPLC MeOH before drying under argon.

4.4. Surface template formation of azPBA-stachyose complex on the C11Alkyne SAM and cavity formation with azOEG

The azPBA:stachyose complex was prepared as previously described by us [60]. Freshly prepared C_{11}Alkyne SAMs were immersed in 1 mL Cu(I) catalyst (10 mol% Cu(II)SO_4, 20 mol% NaAsc, 10 mol% TBTA) containing the azPBA:stachyose complex (0.45 mM) in a DMF: UP H_2O (1.7:1) solution and mixed for intervals of 1, 4, 8 or 24 h. This reaction was quenched by removal of unbound azPBA:stachyose complex by liberal rinsing with HPLC MeOH before drying under argon. The addition of azOEG proceeded by submersing the azPBA:stachyose functionalized substrates in 1 mL of fresh catalyst solution containing 1 mM azOEG for 24 h on a rotary mixer. This reaction was quenched and the template stachyose removed by immersion of the substrates in UP H_2O for 10 min followed by liberal rinsing with UP H_2O. The substrates were then rinsed with HPLC MeOH before drying under argon.

4.5. Ellipsometry characterization of surface thickness

All ellipsometry measurements were made using an alpha-SE ellipsometer (J.A. Woolam). Incidence angle was set at 70° with a wavelength range of 300–900 nm. Calculation of film thickness

was based on a three-phase ambient atmosphere/SAM/Au model with a refractive index set to 1.5 and extinction coefficient (k) at 0.00. Thickness was calculated using CompleteEase software, version 5.26 based on 4 surface measurements on two surfaces (8 total measurements) with error reported from standard deviation between all measurements.

4.6. Contact angle measurements

Contact angle measurements were taken using an Attension Theta contact angle meter (Biolin scientific) using an automated microsyringe to dispense and retract 4 μL water droplets to and from the surface. Advancing and receding angles were obtained from the recording of water drop-out/in at 35 frames per second (FPS) with angles automatically calculated at surface-liquid interface using OneAttension software (version 3.2.2.0). Measurements were taken in triplicate from duplicate SAMs and average reported with error calculated from standard deviation.

4.7. XPS surface elemental characterization

The elemental composition of the C_{11}Alkyne and C_{11}Alkyne-azPBA SAMs was determined by XPS using a Thermo Scientific K-Alpha^{+} XPS spectrophotometer by Harwell XPS laboratories (Cardiff, UK). This used a monochromatic Al K-alpha X-ray source (1486.69 eV) at 72 W with a spot size of 400 μM and a take-off angle at 90°. High resolution peaks were obtained with a pass energy of 50 eV at a step size of 0.1 eV with an energy resolution of 0.5 eV. Samples were run in duplicate with two spots per sample for calculation of error. Peak fitting was completed using casaXPS (version 2.3.18dev1.18) with spectra calibrated using C_{1s} peak charge corrected to 284.8 eV. Relative sensitivity factors for each element were as follows: S_{2p}, 1.68; C_{1s}, 1.0; N_{1s}, 1.8; O_{1s}, 2.93; Au_{4f}, 17.1. The S_{2p} doublet was constrained for peak separation of 1.18 eV and 2:1 area, $S_{2p3/2}$: $S_{2p1/2}$ with equal FWHM. Elemental composition of the C_{11}Alkyne-Pre-azPBA SAM was obtained on a Kratos Supra XPS spectrometer by Harwell XPS laboratory (Cardiff, UK). Elemental composition was obtained using monochromated Al K-alpha X-ray source (1486.69 eV) at 225 W with a spot size of 400 μM and a take-off angle at 90^{O}. High resolution peaks were obtained with a pass energy of 40 eV at a step size of 0.1 eV with an energy resolution of 0.5 eV. Two spots on duplicate samples were analysed. Relative sensitivity factors for each element were as follows: S_{2p}, 0.688; C_{1s}, 0.278; N_{1s}, 0.477; O_{1s}, 0.78; Au_{4f}, 6.25; B_{1s}, 0.159. Peak fitting was conducted as followed for C_{11}Alkyne and azPBA-C_{11}Alkyne XPS spectra.

4.8. SPR saccharide binding studies

SPR binding studies were performed with a Reichert SR7000DC dual channel spectrophotometer with SR7100 autosampler (Reichert technologies, Buffalo, NY, USA). Studies were run at 25 °C, flow rate 25 μl/min, injection 100 μl over 2.5 min with 5 min' equilibration in degassed pH 9.0 ammonium acetate as the running buffer. A baseline was established for each surface by running buffer over the sample at 25 μl/min until a stable baseline was achieved followed by injection of running buffer to provide a blank run. Results were collected with SPR autolink software (Reichert, version 1.1.10-F) and analysed with Scrubber (BioLogic, version 2.0.0.4). To correct for bulk refractive change during saccharide injection, a null saccharide binding surface was prepared substituting azPBA for azBEN (A set of typical SPR curves are shown in Fig. S6).

Credit author statement

J. N. and S. T. conducted the experiments, analysed the data and wrote the manuscript. P.M.M. conceived and designed the study and wrote the manuscript.

Supporting information

Additional details of synthetic procedures and characterization of the SAMs by XPS.

Dedication

This work is dedicated to Professor Sir Fraser Stoddart on the occasion of his 80th birthday.

Declaration of competing interest

The authors declare the following financial interests/personal relationships which may be considered as potential competing interests: Paula Mendes has patent #EP3102303; US 10,775,372; US2020/0371096 issued to Assignee.

Acknowledgments

The authors acknowledge financial support of this work by the EPSRC (EP/K027263/1), ERC (Consolidator Grant 614787), Prostate Cancer UK (RIA17-ST2-020) and ERC Proof-of-Concept (874966).

Abbreviations

MeOH	Methanol
EtOH	Ethanol
UP	Ultra-pure
PBA	Phenylboronic acid
azPBA	Azido-phenylboronic acid
azBEN	Benzyl azide
SAM	Self-assembled monolayer
SPR	Surface plasmon resonance
XPS	X-ray photoelectron spectroscopy
CuAAC	Cu(I)-catalysed azide-alkyne cycloaddition
azOEG	Azido-heptaethylene glycol

Appendix A. Supplementary data

Supplementary data to this article can be found online at https://doi.org/10.1016/j.mtchem.2022.100939.

References

[1] J. Munkley, I. Mills, D. Elliot, The role of glycans in prostate cancer development and progression, Nat. Rev. Urol. 13 (2016) 324–333.
[2] J. Munkley, D.J. Elliott, Hallmarks of glycosylation in cancer, Oncotarget 7 (2016) 35478–35489.
[3] T. Vermassen, M.M. Speeckaert, N. Lumen, S. Rottey, J.R. Delanghe, Glycosylation of prostate specific antigen and its potential diagnostic applications, Clin. Chim. Acta. 413 (2012) 1500–1505.
[4] C. Fu, H. Zhao, Y. Wang, H. Cai, Y. Xiao, Y. Zeng, H. Chen, Tumor-associated antigens: Tn antigen, sTn antigen, and T antigen, HLA 88 (2016) 275–286.
[5] Y. Cao, U. Karsten, G. Otto, P. Bannasch, Expression of MUC1, Thomsen-Friedenreich antigen, Tn, sialosyl-Tn, and alpha2,6-linked sialic acid in hepatocellular carcinomas and preneoplastic hepatocellular lesions, Virchows Arch 434 (1999) 503–509.
[6] J. Kościelak, Diseases of aberrant glycosylation, Acta Biochim. Pol. 42 (1995) 1–10.
[7] J. Mestecky, M. Tomana, Z. Moldoveanu, B.A. Julian, H. Suzuki, K. Matousovic, M.B. Renfrow, L. Novak, R.J. Wyatt, J. Novak, Role of aberrant glycosylation of

IgA1 molecules in the pathogenesis of iga nephropathy, Kidney Blood Press. Res. 31 (2008) 29–37.
[8] K. Kanninen, G. Goldsteins, S. Auriola, I. Alafuzoff, J. Koistinaho, Glycosylation changes in Alzheimer's disease as revealed by a proteomic approach, Neurosci. Lett. 367 (2004) 235–240.
[9] M.L. Montpetit, P.J. Stocker, T.A. Schwetz, J.M. Harper, S.A. Norring, L. Schaffer, S.J. North, J. Jang-Lee, T. Gilmartin, S.R. Head, S.M. Haslam, A. Dell, J.D. Marth, E.S. Bennett, Regulated and aberrant glycosylation modulate cardiac electrical signaling, Proc. Natl. Acad. Sci. U. S. A. 106 (2009) 16517–16522.
[10] S. Saha, R. Murali, A. Pashov, T. Kieber-Emmons, The potential role of solvation in antibody recognition of the lewis y antigen, Monoclon. Antib. Immunodiagn. Immunother. 34 (2015) 295–302.
[11] O. Blixt, O.I. Lavrova, D.V. Mazurov, E. Cló, S.K. Kračun, N.V. Bovin, A.V. Filatov, Analysis of Tn antigenicity with a panel of new IgM and IgG1 monoclonal antibodies raised against leukemic cells, Glycobiology 22 (2012) 529–542.
[12] C.R. MacKenzie, T. Hirama, S.J. Deng, D.R. Bundle, S.A. Narang, N.M. Young, Analysis by surface plasmon resonance of the influence of valence on the ligand binding affinity and kinetics of an anti-carbohydrate antibody, J. Biol. Chem. 271 (1996) 1527–1533.
[13] C.T. Yuen, C.K. Gee, C. Jones, High-performance liquid chromatographic profiling of fluorescent labelled N-glycans on glycoproteins, Biomed. Chromatogr. 16 (2002) 247–254.
[14] H.J. An, S. Miyamoto, K.S. Lancaster, C. Kirmiz, B. Li, K.S. Lam, G.S. Leiserowitz, C.B. Lebrilla, Profiling of glycans in serum for the discovery of potential biomarkers for ovarian cancer, J. Proteome Res. 5 (2006) 1626–1635.
[15] J. Bones, S. Mittermayr, N. O'Donoghue, A. Guttman, P.M. Rudd, Ultra performance liquid chromatographic profiling of serum N-glycans for fast and efficient identification of cancer associated alterations in glycosylation, Anal. Chem. 82 (2010) 10208–10215.
[16] E. Song, A. Mayampurath, C.Y. Yu, H. Tang, Y. Mechref, Glycoproteomics: identifying the glycosylation of prostate specific antigen at normal and high isoelectric points by LC-MS/MS, J. Proteome Res. 13 (2014) 5570–5580.
[17] L. Han, C.E. Costello, Mass spectrometry of glycans, Biochem 78 (2013) 710–720.
[18] L. Duan, Y. Zhao, Selective binding of folic acid and derivatives by imprinted nanoparticle receptors in water, Bioconjug. Chem. 29 (2018) 1438–1445.
[19] R.A. Almotiri, K.J. Ham, V.M. Vijayan, S.A. Catledge, Molecularly imprinted polyacrylamide with fluorescent nanodiamond for creatinine detection, Materials 12 (2019).
[20] F.L. Dickert, H. Besenböck, M. Tortschanoff, Molecular imprinting through van der Waals interactions: fluorescence detection of PAHs in water, Adv. Mater. 10 (1998) 149–151.
[21] F. Breton, R. Delépée, L.A. Agrofoglio, Molecular imprinting of AMP by an ionic-noncovalent dual approach, J. Sep. Sci. 32 (2009) 3285–3291.
[22] N. Suda, H. Sunayama, Y. Kitayama, Y. Kamon, T. Takeuchi, Oriented, molecularly imprinted cavities with dual binding sites for highly sensitive and selective recognition of cortisol, R. Soc. Open Sci. 4 (2017).
[23] H. Asanuma, T. Hishiya, M. Komiyama, Efficient separation of hydrophobic molecules by molecularly imprinted cyclodextrin polymers, J. Incl. Phenom. 50 (2004) 51–55.
[24] M. Arifuzzaman, W. Zhao, Y. Zhao, Surface ligands in the imprinting and binding of molecularly imprinted cross-linked micelles, Supramol. Chem. 30 (2018) 929–939.
[25] P. Mitchell, S. Tommasone, S. Angioletti-Uberti, J. Bowen, P.M. Mendes, Precise generation of selective surface-confined glycoprotein recognition sites, ACS Appl. Bio Mater. 2 (2019) 2617–2623.
[26] A. Stephenson-Brown, H.C. Wang, P. Iqbal, J.A. Preece, Y. Long, J.S. Fossey, T.D. James, P.M. Mendes, Glucose selective Surface Plasmon Resonance-based bis-boronic acid sensor, Analyst 138 (2013) 7140–7145.
[27] A. Stephenson-Brown, A.L. Acton, J.A. Preece, J.S. Fossey, P.M. Mendes, Selective glycoprotein detection through covalent templating and allosteric click-imprinting, Chem. Sci. 6 (2015) 5114–5119.
[28] H. Wang, J. Yi, D. Velado, Y. Yu, S. Zhou, Immobilization of carbon dots in molecularly imprinted microgels for optical sensing of glucose at physiological pH, ACS Appl. Mater. Interfaces. 7 (2015) 15735–15745.
[29] S.A. Piletsky, H.S. Andersson, I.A. Nicholls, Combined hydrophobic and electrostatic interaction-based recognition in molecularly imprinted polymers, Macromolecules 32 (1999) 633–636.
[30] Y. Kim, J. Lee, I.S. Shin, Advanced method for fabrication of molecularly imprinted mesoporous organosilica with highly sensitive and selective recognition of glyphosate, Sci. Rep. 9 (2019) 1–8.
[31] Y. Kanekiyo, M. Sano, R. Iguchi, S. Shinkai, Novel nucleotide-responsive hydrogels designed from copolymers of boronic acid and cationic units and their applications as a QCM resonator system to nucleotide sensing, J. Polym. Sci. Part A Polym. Chem. 38 (2000) 1302–1310.
[32] N.W. Turner, C.W. Jeans, K.R. Brain, C.J. Allender, V. Hlady, D.W. Britt, From 3D to 2D: a review of the molecular imprinting of proteins, ((n.d.)).
[33] A. Bossi, S.A. Piletsky, E.V. Piletska, P.G. Righetti, A.P.F. Turner, Surface-grafted molecularly imprinted polymers for protein recognition, Anal. Chem. 73 (2001) 5281–5286.
[34] S.A. Piletsky, E.V. Piletska, A. Bossi, K. Karim, P. Lowe, A.P.F. Turner, Substitution of antibodies and receptors with molecularly imprinted polymers in enzyme-linked and fluorescent assays, Biosens. Bioelectron. 16 (2001) 701–707.
[35] S.D. Bull, M.G. Davidson, J.M.H. Van Den Elsen, J.S. Fossey, A.T.A. Jenkins, Y.B. Jiang, Y. Kubo, F. Marken, K. Sakurai, J. Zhao, T.D. James, Exploiting the reversible covalent bonding of boronic acids: recognition, sensing, and assembly, Acc. Chem. Res. 46 (2013) 312–326.
[36] N.W. Turner, X. Liu, S.A. Piletsky, V. Hlady, D.W. Britt, Recognition of conformational changes in β-lactoglobulin by molecularly imprinted thin films, Biomacromolecules 8 (2007) 2781–2787.
[37] J. Rick, T.C. Chou, Enthalpy changes associated with protein binding to thin films, Biosens. Bioelectron. 20 (2005) 1878–1883.
[38] S.A. Piletsky, E.V. Piletska, B. Chen, K. Karim, D. Weston, G. Barrett, P. Lowe, A.P.F. Turner, Chemical grafting of molecularly imprinted homopolymers to the surface of microplates. Application of artificial adrenergic receptor in enzyme-linked assay for β-agonists determination, Anal. Chem. 72 (2000) 4381–4385.
[39] L. Gu, X. Jiang, Y. Liang, T. Zhou, G. Shi, Double recognition of dopamine based on a boronic acid functionalized poly(aniline-co-anthranilic acid)-molecularly imprinted polymer composite, Analyst 138 (2013) 5461–5469.
[40] L. Zhang, C. Zhu, C. Chen, S. Zhu, J. Zhou, M. Wang, P. Shang, Determination of kanamycin using a molecularly imprinted SPR sensor, Food Chem. 266 (2018) 170–174.
[41] Y. Ben-Amram, M. Riskin, I. Willner, Selective and enantioselective analysis of mono- and disaccharides using surface plasmon resonance spectroscopy and imprinted boronic acid-functionalized Au nanoparticle composites, Analyst 135 (2010) 2952–2959.
[42] H. Matsumoto, H. Sunayama, Y. Kitayama, E. Takano, T. Takeuchi, Site-specific post-imprinting modification of molecularly imprinted polymer nanocavities with a modifiable functional monomer for prostate cancer biomarker recognition, Sci. Technol. Adv. Mater. 20 (2019) 305–312.
[43] V.V. Rostovtsev, L.G. Green, V.V. Fokin, K.B. Sharpless, A stepwise huisgen cycloaddition process: copper(I)-catalyzed regioselective "ligation" of azides and terminal alkynes, Angew. Chem. Int. Ed. 41 (2002) 2596–2599.
[44] M. Trujillo, C. Hull-Crew, A. Outlaw, K. Stewart, L. Taylor, L. George, A. Duensing, B. Tracey, A. Schoffstall, Green methodologies for copper(I)-catalyzed azide-alkyne cycloadditions: a comparative study, Molecules 24 (2019) 1–12.
[45] L.K. Rasmussen, B.C. Boren, V.V. Fokin, Ruthenium-catalyzed cycloaddition of aryl azides and alkynes, Org. Lett. 9 (2007) 5337–5339.
[46] F. Friscourt, G.J. Boons, One-pot three-step synthesis of 1,2,3-triazoles by copper-catalyzed cycloaddition of azides with alkynes formed by a Sonogashira cross-coupling and desilylation, Org. Lett. 12 (2010) 4936–4939.
[47] Y. Li, C. Cai, Click chemistry-based functionalization on non-oxidized silicon substrates, Chem. Asian J. 4 (6) (2011) 2592–2605.
[48] R. Chelmowski, D. Kafer, S.D. Köster, T. Klasen, T. Winkler, A. Terfort, N. Metzler-Nolte, C. Wöll, Postformation modification of SAMs: using click chemistry to functionalize organic surfaces, Langmuir 25 (2009) 11480–11485.
[49] R.D. Rohde, H.D. Agnew, W.S. Yeo, R.C. Bailey, J.R. Heath, A non-oxidative approach toward chemically and electrochemically functionalizing Si(111), J. Am. Chem. Soc. 128 (2006) 9518–9525.
[50] S. Ciampi, T. Bo, K.A. Kilian, M. James, J.B. Harper, J.J. Gooding, Functionalization of acetylene-terminated monolayers on Si (100) surfaces : a click chemistry approach, Langmuir (2007) 9320–9329.
[51] J. Chen, B. Chang, S. Oyola-Reynoso, Z. Wang, M. Thuo, Quantifying gauche defects and phase evolution in self-assembled monolayers through sessile drops, ACS Omega 2 (2017) 2072–2084.
[52] Q. Guo, F. Li, Self-assembled alkanethiol monolayers on gold surfaces: resolving the complex structure at the interface by STM, Phys. Chem. Chem. Phys. 16 (2014) 19074–19090.
[53] Q. Chi, J. Zhang, J. Ulstrup, Surface microscopic structure and electrochemical rectification of a branched alkanethiol self-assembled monolayer, J. Phys. Chem. B. 110 (2006) 1102–1106.
[54] V. Chechik, H. Schönherr, G.J. Vancso, C.J.M. Stirling, Self-assembled monolayers of branched thiols and bisulfides on gold: surface coverage, order and chain orientation, Langmuir 14 (1998) 3003–3010.
[55] L. Ramin, A. Jabbarzadeh, Odd-even effects on the structure, stability, and phase transition of alkanethiol self-assembled monolayers, Langmuir 27 (2011) 9748–9759.
[56] M. James, S. Ciampi, T.A. Darwish, T.L. Hanley, S.O. Sylvester, J.J. Gooding, Nanoscale water condensation on click-functionalized self-assembled monolayers, Langmuir 27 (2011) 10753–10762.
[57] F. Wei, W. Wang, Y. Ma, C.H. Tung, Z. Xu, Regioselective synthesis of multi-substituted 1,2,3-triazoles: moving beyond the copper-catalyzed azide-alkyne cycloaddition, Chem. Commun. 52 (2016) 14188–14199.
[58] X. Wu, Z. Li, X.X. Chen, J.S. Fossey, T.D. James, Y.B. Jiang, Selective sensing of saccharides using simple boronic acids and their aggregates, Chem. Soc. Rev. 42 (2013) 8032–8048.
[59] L. Patrone, V. Gadenne, S. Desbief, Single and binary self-assembled monolayers of phenyl-and pentafluorophenyl-based silane species, and their phase separation with octadecyltrichlorosilane, Langmuir 26 (2010) 17111–17118.
[60] S. Tommasone, Y.K. Tagger, P.M. Mendes, Targeting oligosaccharides and glycoconjugates using superselective binding scaffolds, Adv. Funct. Mater. 30 (2020) 5–10.
[61] K.N. Turhan, F. Sahbaz, A. Güner, A spectrophotometric study of hydrogen bonding in methylcellulose-based edible films plasticized by polyethylene glycol, J. Food Sci. 66 (2001) 59–62.
[62] S. Tommasone, F. Allabush, Y.K. Tagger, J. Norman, M. Kopf, J.H.R. Tucker, P.M. Mendes, The challenges of glycan recognition with natural and artificial receptors, Chem. Soc. Rev. 48 (2019) 5488–5505.